The Effect of Sodium Thiosulfate on Cytotoxicity of a Diimine Re(I) Tricarbonyl Complex

*Miles S. Capper,[a] Alejandra Enriquez Garcia,[a] Barry Lai,[b] Baiwen O. Wang,[a] Benjamin S. Gelfand,[a] Carrie S. Shemanko,[c] and Farideh Jalilehvand [a,]**

[a] Department of Chemistry, University of Calgary, Calgary, Alberta, T2N 1N4, Canada

[b] Advanced Photon Source, X-ray Science Division, Argonne National Laboratory, Argonne, USA

[c] Department of Biological Sciences, University of Calgary, Calgary, Alberta, T2N 1N4, Canada

Keywords: Re(I) tricarbonyl complexes, Thiosulfate, Cytotoxicity, X-ray Fluorescence Microscopy

Abstract

Recently, diimine Re(I) tricarbonyl complexes have attracted great interest due to their promising cytotoxic effects. Here, we compare the cytotoxicity and cellular uptake of two Re(I) compounds *fac*-[(Re(CO)$_3$(bpy)(H$_2$O)](CF$_3$SO$_3$) (**1**) and Na(*fac*-[(Re(CO)$_3$(bpy)(S$_2$O$_3$)])·H$_2$O (bpy = 2,2'-bipyridine) (**2**). The Re-thiosulfate complex in **2** was characterized in two solvated crystal structures {Na(*fac*-[Re(CO)$_3$(bpy)(S$_2$O$_3$)]) · 1.75H$_2$O · C$_2$H$_5$OH}$_4$ (**2** + 0.75H$_2$O + C$_2$H$_5$OH)$_4$ and (*fac*-[Re(CO)$_3$(bpy)(H$_2$O)]) (*fac*-[Re(CO)$_3$(bpy)(S$_2$O$_3$)])·4H$_2$O (**3**). The cytotoxicity of **1** and **2** was tested in the MDA-MB-231 breast cancer cell line and compared with that of cisplatin. The cellular localization of the Re(I) complexes was investigated using synchrotron-based X-ray fluorescence microscopy (XFM). The results show that replacement of the aqua ligand with thiosulfate renders the complex less toxic most likely by distrupting its cellular entry. Therefore, thiosulfate could potentially have a similar chemoprotective effect against diimine *fac*-Re(CO)$_3$ complexes as it has against cisplatin.

Introduction

The treatment of cancer using metal-based drugs has risen to prominence since the discovery of cisplatin in 1965 by Barnet Rosenberg.[1] However, dose-limiting toxic side effects, as well as the development of resistance mechanisms, reduce the effectiveness of cisplatin.[2, 3] Even though merely 1% of the administered cisplatin reaches to the site of action within the cells,[4] its dosage cannot be simply increased, since overdose of cisplatin may lead to significant morbidity and/or mortality.[2] Some side effects of cisplatin are attributed to its ease of aquation and high lability of Pt-aqua bonds,[5, 6] which facilitates cisplatin binding to certain enzymes and their deactivation.[7] Cisplatin and its hydrolysis products, such as the highly toxic monoaqua complex *cis*-$[Pt(NH_3)_2(H_2O)Cl]^+$, can induce oxidative stress, damaging cells and tissues. Increased level of reactive oxygen species (ROS) upon cisplatin exposure may occur through different pathways, including cisplatin reaction with glutathione, which plays an important role in protecting cells from ROS, as well as cisplatin binding to mitochondrial DNA leading to mitochondrial dysfunction. [8, 9]

Several human studies show the chemoprotective effectiveness of sodium thiosulfate ($Na_2S_2O_3$, STS) against cisplatin and carboplatin, allowing administration of higher doses of cisplatin to be administered in patients. Delayed administration of STS in large excess (up to 1000-fold) after cisplatin or carboplatin allows enough time for their chemotherapeutic effect to occur, while reducing the incidence and severity of some of the side effects such as hearing loss due to ototoxicity.[10-17] It has been also used to treat acute renal failure developed following accidental cisplatin overdose.[18]

Thiosulfate is an endogenous ion with antioxidant properties; therefore, it can reduce cisplatin toxic effects by quenching ROS.[9, 16] Moreover, cisplatin and its hydrolysis products can

form, with sodium thiosulfate, biologically inactive complexes which have no chemotherapeutic capacity.[19, 20] It has been observed that patients who received cisplatin through rapid intravenous infusion, a day later had 65-98% of the platinum bound to plasma proteins in their blood, which lowers Pt urinary excretion and increases its tissue deposition.[7] *In vitro* studies show that formation of such thiosulfate complexes reduces the binding of cisplatin hydrolysis products to human plasma proteins,[21] and decreases the amount of the highly reactive complex, *cis*-$[Pt(NH_3)_2(H_2O)Cl]^+$, in the blood plasma.[16, 22] Although the mechanism of action of sodium thiosulfate *in vivo* is not fully understood, yet it clearly has some chemoprotective effect against cisplatin toxicity.

Many efforts are underway to explore other metal-based chemotherapeutic agents to achieve higher selectivity and fewer side effects. The reactivity of transition metal complexes towards biomolecules can be modified by varying their geometries, coordination numbers, charge, nature of coordinated ligands, and redox properties, allowing specific design of complexes with anticancer activity.[23] Earlier investigations of Ru(II) and Re(I)-based complexes have shown promising results.[24-29] Their ligand exchange reactions are generally slow due to their kinetically inert low spin d^6 configuration.

More recently, Re(I) tricarbonyl diimine complexes with the general formula *fac*-$[Re(CO)_3(N,N)(X)]^{0/+}$ (*N,N* = a bidentate diimine such as 2,2'-bipyridine (bpy) and 1,10-phenanthroline (phen); an ancillary ligand X = halides, H_2O, pyridine derivatives, phosphines (PR_3)) have attracted interest due to their anti-proliferative, photophysical and luminescence imaging properties.[30] Such complexes show cytotoxicity in a range of human cancer cell lines, highlighting their potential as chemotherapeutic agents.[31-37] The mechanism of action in which the complexes initiate cell death is not yet fully understood, although in many cases such complexes have been localized in the cytoplasm and mitochondria.[30, 38] The emissive properties of rhenium-

based complexes in the visible region facilitate their cellular localization with confocal and fluorescence microscopy. However, such optical studies of the intracellular distribution and drug activity of the Re(I) tricarbonyl complexes can be hampered by quenching when inside the cell.[32, 39-41]

In such cases, synchrotron-based X-ray fluorescence microscopy (XFM) is particularly useful since it involves X-ray fluorescence emission. This occurs when an atom absorbs X-rays with certain energies, leading to the ejection of an inner-shell electron. When an electron from higher energy level relaxes, element-specific fluorescent photons are emitted.[42] The fluorescent photons can be detected by an energy-dispersive detector, allowing quantification of a particular element in a sample.[42] This technique has been recently used to show the *in vitro* stability and intracellular distribution of two rhenium(I) complexes: the neutral *fac*-[$Re(CO)_3$(phen)(5-(4-iodophenyl)tetrazolate)] and the cationic *fac*-[$Re(CO)_3$(dmphen)(*p*-tolylisonitrile)]$^+$ (dmphen = 2,9-dimethyl-1,10-phenantroline), which show cytotoxic activity towards a variety of cell lines.[43, 44] Using XFM, we were able to explain the significant changes in cytotoxicity of *fac*-[$Re(CO)_3$(bpy)(H_2O)](CF_3SO_3) (**1**) [45] as a result of reduced cellular uptake of the product when the aqua ligand is replaced with cysteine (H_2Cys), forming *fac*-[$Re(CO)_3$(bpy)(HCys)].[46]

Here, we present the synthesis and structural characterization of the thiosulfate complex in the compound Na(*fac*-[$Re(CO)_3$(bpy)(S_2O_3)])·H_2O (**2**), obtained from the reaction of **1** with $Na_2S_2O_3$ in aqueous solution. We report the crystal structures of {Na(*fac*-[$Re(CO)_3$(bpy)(S_2O_3)])·1.75H_2O·C_2H_5OH}$_4$ (**2**+0.75H_2O+C_2H_5OH)$_4$ and (*fac*-[$Re(CO)_3$(bpy)(H_2O)])(*fac*-[$Re(CO)_3$(bpy)(S_2O_3)])·4H_2O (**3**). Dissolving **1** and **2** in water generates cationic *fac*-[$Re(CO)_3$(bpy)(H_2O)]$^+$ and anionic *fac*-[$Re(CO)_3$(bpy)(S_2O_3)]$^-$ complexes.

We assessed the cytotoxicity of both complexes against the MDA-MB-231 breast cancer cell line, and probed their cellular distribution using XFM. Our results show that substitution of the aqua ligand with thiosulfate reduces the toxicity of the Re(I) complex by inhibiting its cellular uptake. Therefore, a similar chemoprotective effect of sodium thiosulfate could be expected against diimine rhenium(I) tricarbonyl aqua complexes as for cisplatin.

Experimental Section

Materials. Rhenium pentacarbonyl chloride (98%), 2,2'-bipyridine and hydrated sodium thiosulfate were obtained from Sigma Aldrich and used without further purification. Dry toluene was prepared under argon atmosphere by refluxing (110 ºC) in presence of benzophenone and Na metal.[47] *fac*-[$Re(CO)_3(bpy)(H_2O)$](CF_3SO_3) (**1**) was prepared from *fac*-[$Re(CO)_3(bpy)Cl$] as previously described.[46, 48, 49]

Cell culture. MDA-MB-231 breast cancer cells (American Type Culture Collection; ATCC) were genetically validated and used within 6 months of testing. Cells were cultured as a monolayer with Dulbecco's Modified Eagles Medium (DMEM) (Invitrogen/Gibco) supplemented with heat-inactivated foetal bovine serum (10% v/v; Sigma Life Sciences), L-glutamine (2 mM, Invitrogen), Penicillin (100 units/mL), Streptomycin (100 µg/mL) at 37 ºC in a 5% CO_2-humidified incubator and were sub-cultured every 3–4 days.

Synthesis

*Na(fac-[$Re(CO)_3(bpy)(S_2O_3)$])·H_2O (**2**)*

Solid sodium thiosulfate (4.21 mmol) was added to a completely dissolved yellow solution of **1** (0.42 mmol) in 20 mL water; the suspension was left to stir for 48 h at room temperature. Excess

solid sodium thiosulfate was removed by filtering the solution; the filtrate was then concentrated through rotary evaporation at 45 ºC and left in the fridge in a sealed container for 48 h. Yellow needle-shaped crystals formed, which were collected using a polyethersulfone (PES) membrane filter and washed with water and ether. Elemental anal. calcd for Na(*fac*-[$Re(CO)_3(bpy)(S_2O_3)$])·H_2O ($ReC_{13}H_{10}N_2O_7S_2Na$): %C, 26.94; %H, 1.74; %N, 4.83 (3.1% H_2O). Found: %C, 27.12; %H, 1.46; %N, 4.88 (TGA: 3.0% H_2O); yield: 67%. ^{1}H NMR (600 MHz, D_2O*)* δ 9.05 (d, *J* = 5.4 Hz, 2H), 8.41 (d, *J* = 8.2 Hz, 2H), 8.16 (td, *J* = 7.8, 1.5 Hz, 2H), 7.61 (td, *J* = 6.6, 1.2 Hz, 2H). ^{13}C {^{1}H} NMR (600 MHz, D_2O), 198.12 (CO_{eq}), 191.59 (CO_{ax}), 156.0 (C1, C1′), 153.9 (C3, C3′), 140.0 (C5, C5′), 127.6 (C4, C4′), 124.1 (C6, C6′). IR $\tilde{\nu}_{co}$ = 2018, 1914, 1884 cm^{-1}; see Figures S1 (b) and S2-S4. The single crystal taken from its mother liquor (ethanol/ pentane) for crystallography had the composition Na(*fac*-[$Re(CO)_3(bpy)(S_2O_3)$]) ·1.75H_2O · C_2H_5OH (**2** + 0.75H_2O + C_2H_5OH). Using water/pentane as the solvent system, led to single crystals with different composition (*see below*).

Physical Measurements and Methods

Single Crystal X-ray Diffraction.

Single crystals were grown using the vapor diffusion method, for (**2** + 0.75H_2O + C_2H_5OH) in EtOH/pentane and for *fac*-[$Re(CO)_3(bpy)(H_2O)$])(*fac*-[$Re(CO)_3(bpy)(S_2O_3)$])·4H_2O (**3**) with water/pentane as solvent. Suitable crystals were selected and mounted on a glass loop using Paratone oil. Data collection was performed at 173 K on a Bruker Smart diffractometer equipped with an Incoatec Microfocus (graphite monochromated Cu K_α, λ = 1.54178 Å) and an APEX II CCD detector. The diffractions spots were integrated and scaled with SAINT[50] and the space groups were determined with XPREP.[51] Using Olex2,[52] the structures were solved with the

ShelXT[53] structure solution program using Intrinsic Phasing and refined with the ShelXL[54] refinement package using Least Squares minimization. Hydrogen atoms bound to heteroatoms were placed in geometrically calculated positions to maximize hydrogen bonding interactions.

Cell Viability.

MDA-MB-231 breast cancer cells were seeded 7500 cells per well in black-walled 96-well plates and cultured for 48 h. Stock solutions of **1** and **2** were freshly prepared in DMEM. Drug exposure periods were 24 or 48 h, as indicated. Cells were washed with phosphate buffer saline (PBS). The media was replaced with that containing 10% v/v alamarBlue reagent and the cells were incubated at 37 ºC in a 5% CO_2-humidified incubator. After 2.5 h incubation, followed by excitation (λ = 565-575 nm), the emission wavelengths (λ = 585-595 nm) were monitored by a SpectraMax M2e Multi-detection Readers. Cell viability is reported as a percentage of the emission from cells treated with either **1** or **2** with respect to the vehicle control (DMEM) and were determined by three independent experiments using nine biological replicates; their standard deviations were calculated. IC_{50} values were determined by curve fitting-plots of cell viability (%) vs. log of drug concentration.

XFM Sample Preparation.

Fresh stock solutions of **1** (800 μM) and **2** (3200 μM) were prepared in DMEM and diluted with DMEM to the treatment concentration of 20 μM. Samples for XFM imaging were prepared by growing cancer cells on 1.5 x 1.5 mm x 500 nm silicon nitride windows (Silson, UK) in 6-well plates as described previously.[55] The plates were seeded at 225,000 cells per well; cells were allowed to attach to the Si_3N_4 windows at 37 ºC in a 5% CO_2-humidified incubator for 24 h prior to treatment. Cells were then treated for 6 h with 20 μM solutions of **1** and **2**, or with DMEM as a

vehicle control. At the end of the treatment time, the medium was removed and the cells washed with Dulbecco's PBS (D-PBS). The cells were then fixed with 4% paraformaldehyde (prepared fresh in D-PBS) solution for 1 h in a 37 ºC in a 5% CO_2-humidified incubator. The cells fixed on Si_3N_4 windows were then washed twice with ammonium acetate in Milli-Q water (100 mM) to remove excess fixatives (and NaCl) and left to dry overnight.[56, 57]

XFM Data Collection.

Elemental distribution maps of single cells (Figures S5 a-c) were recorded on beamline 2-ID-D at the Advanced Photon Source (APS), Argonne National Laboratory, Illinois, USA. The X-ray beam was tuned using a double crystal monochromator to an incident energy of 12.8 keV to generate the Re L_β emission line (E= 10,010.0 eV). The beam was focused to a spot size of 0.35 μm on the sample using two Fresnel zone plates. A single element silicon drift energy dispersive detector (Vortex EX, SII Nano-technology) was used to collect the X-ray fluorescent spectra from the samples that were kept under He atmosphere at 75º to the incident beam. All elemental maps were recorded using the step-scan mode, with 0.5 μm spatial resolution (step-size) and 1 s dwell time. Four to five cells per sample were selected for imaging, using an optical microscope.

The fitting of raw fluorescence emission spectra to Gaussian line shapes at each spatial point allowed for the generation of elemental maps (in units of μg cm^{-2}), as well as regions of interest (ROIs).[58, 59] Rhenium images were obtained by fitting its L_β emission line (10010.0 eV), since its L_α line (8586.2 eV) almost overlaps with the Zn K_α (8638.9 eV) fluorescence line (Figure S6). Quantification was performed through comparison of X-ray fluorescence intensity to the thin-film standards, NBS-1832 and NBS-1833, from the National Bureau of Standards (Gaithersburg, MD). The analysis was performed using MAPS software.[59, 60]

Results and Discussion

Characterization of the Re(I) thiosulfate complex (2)

Reaction of *fac*-[$Re(CO)_3(bpy)(H_2O)$](CF_3SO_3) (**1**) with excess $Na_2S_2O_3$ in aqueous solution led to the formation of crystalline Na(*fac*-[$Re(CO)_3(bpy)(S_2O_3)$])·H_2O (**2**). Both compounds **1** and **2** displayed good solubility in water. Scheme 1 provides an overview for syntheses of **2**.

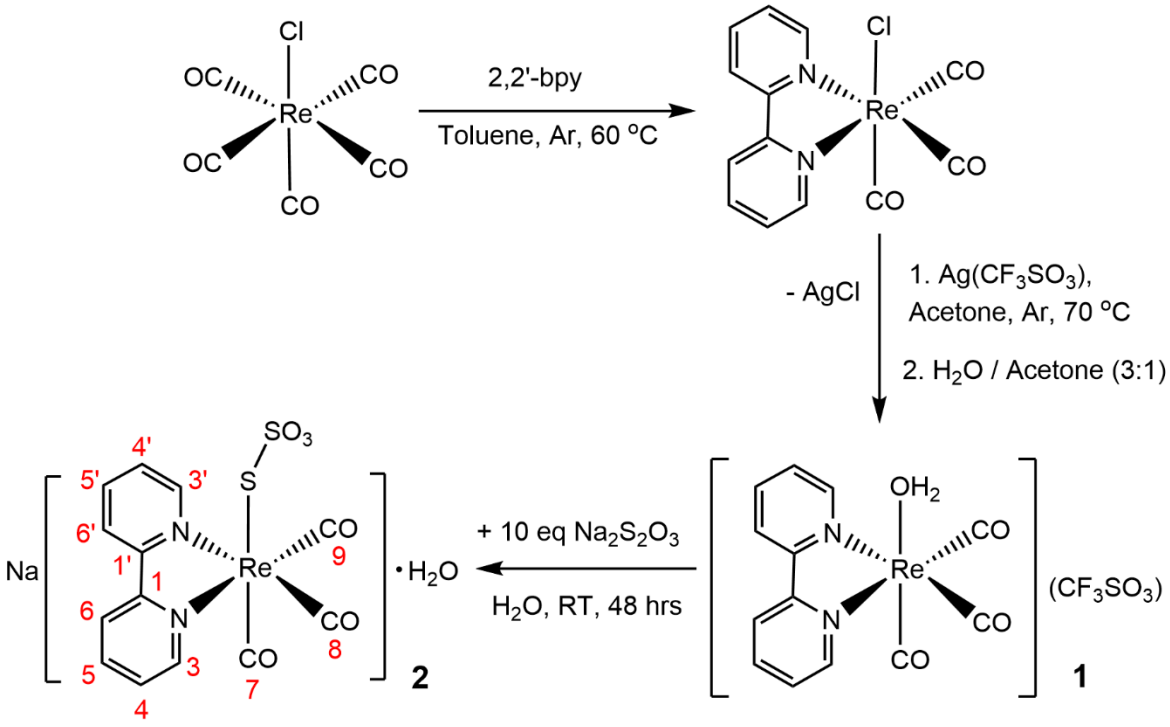

Scheme 1. Synthetic route for Na(*fac*-[$Re(CO)_3(bpy)(S_2O_3)$])·H_2O (**2**). The numbers in red refer to the C atoms associated with ^{13}C NMR signals, as described in the *Experimental Section*.

To prepare single crystals of **2** using the vapour diffusion method, we initially chose water as the solvent and pentane as the precipitant. Long needle-shaped crystals with the formula (*fac*-[$Re(CO)_3(bpy)(H_2O)$])(*fac*-[$Re(CO)_3(bpy)(S_2O_3)$])·$4H_2O$ (**3**) formed almost instantly at lower

temperature (4 ºC). Solving the crystal structure of **3** was challenging, as the chemical formula of this ion pair did not match that expected for **2**. When EtOH was used as solvent of **2** under similar conditions, small single crystals of another solvated compound were grown with the formula $\{Na(fac\text{-}[Re(CO)_3(bpy)(S_2O_3)])\cdot 1.75H_2O\cdot C_2H_5OH\}_4$ (**2** + $0.75H_2O$ + $C_2H_5OH)_4$. Crystal data and refinement parameters for both Re(I) crystal structures are presented in Table S1, with selected interatomic distances and bond angles reported in Tables S2-S5. The atomic arrangements in the crystal structures are displayed in Figures 1 and 2.

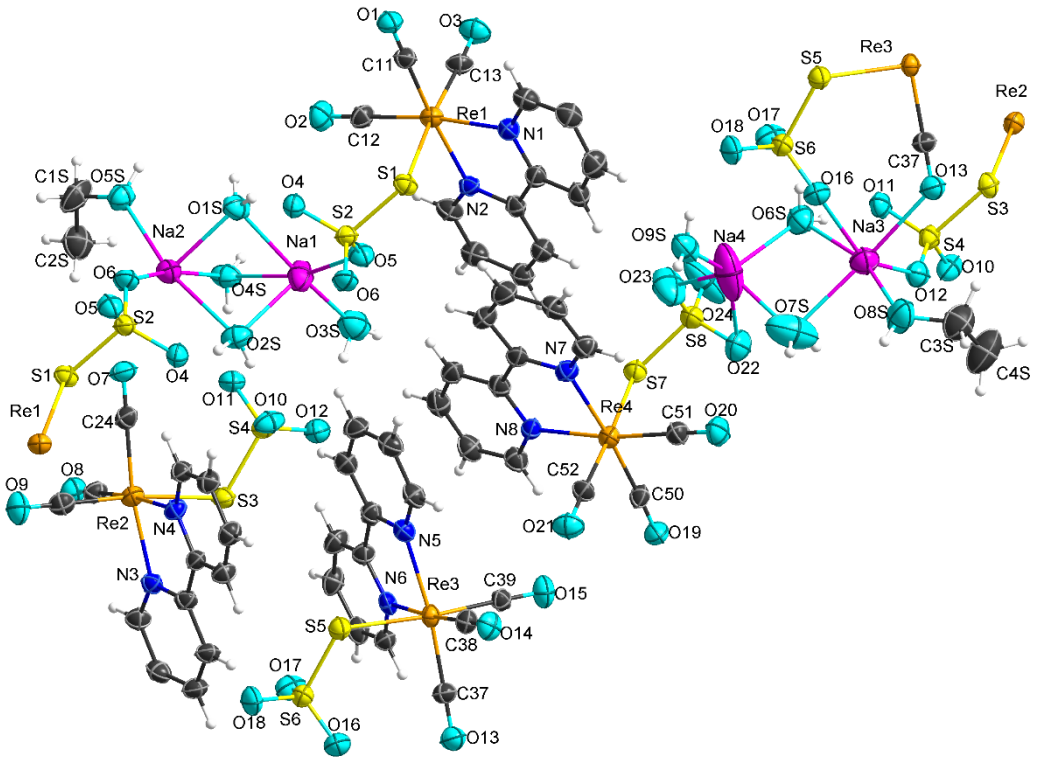

Figure 1. Crystal Structure of $\{Na(fac\text{-}[Re(CO)_3(bpy)(S_2O_3)])\cdot 1.75H_2O\cdot C_2H_5OH\}_4$ (**2** + $0.75H_2O$ + $C_2H_5OH)_4$. Ellipsoids are drawn at the 50% probability level. H atoms have spherical representation.

The crystal structure of the solvated compound **2** contains four crystallographically different Re(I) centres, with the Re-S bond lengths in the narrow range between 2.511(2) to

2.525(2) Å (Table S2). This is in agreement with the reported range for Re-S bond distances in similar *fac*-[Re(CO)$_3$(*N,N*)(X)] complexes with varying S-donor ancillary ligands including thiolates, thiones and thiocarbamates (See Table S6).[61-63] The replacement of the aqua ligand in **1** with thiosulfate in **2** appeared to slightly increase the bond length of the axially bound CO ligand from Re-C$_{axial}$ 1.88(1) Å in **1**[49] to 1.906(7) – 1.933(7) Å in **2** (see Table S2), but did not significantly impact other Re-ligand distances. Similar complexes with other ancillary ligands also display little variance in the Re-ligand bond lengths.[45] Note the bridging water molecules between the Na^+ ions, which together with hydrogen bonds hold the Re-complexes together.

In the ionic *fac*-[Re(CO)$_3$(bpy)(S$_2$O$_3$)]$^-$ complex in the crystal structure of **3** (shown in Figure 2), the Re-S distance of 2.481(3) Å is considerably shorter, and consequently the *trans* carbonyl Re-C bond length 1.941(11) Å is longer than the corresponding distances in **2**.

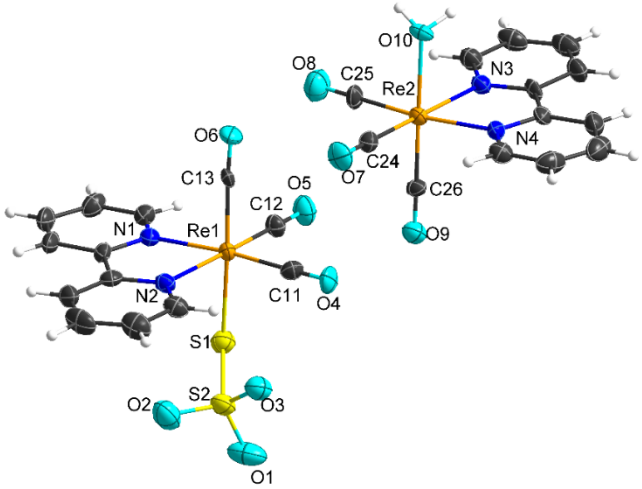

Figure 2. Crystal Structure of (*fac*-[Re(CO)$_3$(bpy)(H$_2$O)])(*fac*-[Re(CO)$_3$(bpy)(S$_2$O$_3$)])·4H$_2$O (**3**) Non-coordinated water molecules have been omitted for clarity. Ellipsoids are drawn at the 50% probability level. H atoms have spherical representation.

The Re-thiosulfate complex in **2** was further characterized using ^{1}H, ^{13}C NMR and FT-IR spectroscopy, as well as electrospray ionization mass spectrometry (ESI-MS). Its ESI-mass

spectrum in (-) ion mode displayed peaks at -*m/z* = 382.87 and 538.94 amu for $[Re(CO)_3(S_2O_3)]^-$ and $[Re(CO)_3(bpy)(S_2O_3)]^-$, respectively. Also, intense mass peaks at +*m/z* = 427.01, 540.95 and 557.98 amu, corresponding to $[Re(CO)_3(bpy)]^+$, $[Re(CO)_3(bpy)(S_2O_3) + 2H^+]^+$ and $[Re(CO)_3(bpy)(S_2O_3) + H^+ + NH_4^+]^+$, respectively, were detected in the (+) ion mode, with isotopic patterns characteristic of Re and S atoms (see Figure S3, Table S7).

The ^1H and ^{13}C NMR signals observed for **2** were slightly shifted up-field in comparison to **1**; see Figures S1 (a) and (b). This shift can be explained based on the increased electron density experienced by the Re(I) ion, when the thiosulfate group replaces the aqua ligand. Similarly, a shift to lower frequencies is observed when comparing the characteristic C≡O stretching bands of **1** and **2** in their FT-IR spectra, which occur at 2033 and 2018 cm^{-1}, respectively, corresponding to the totally symmetric in-phase ν(CO) vibrational mode, denoted as A′(1) (Figure S2).[64] This reduction in the vibrational frequency is consistent with the increase in electron density on the Re(I) ions in **2**, which is π-back donated to the π* antibonding orbital of the carbonyl groups, thus weakening the C≡O bond. While the asymmetric stretching mode of the equatorial C≡O groups (A″) and the totally symmetric out-of-phase mode A′(2) of the C≡O ligands form a single broad band at 1914 cm^{-1} in **1**, adjacent peaks can be distinguished at 1914 and 1884 cm^{-1} for **2**, with the A′(2) mode at the lower frequency (Figure S2). Separation of these two vibrational bands is typically observed in complexes bearing halide, *O*- or *P*- donor ancillary ligands - although this is not the case for **1**, while one broad band occurs for the *N*-donor ancillary ligands, i.e. $Re(CO)_3(N,N)(N)$ complexes with pseudo C_{3v} symmetry.[64] The observed separation of the A′(2) and A″ vibrational modes in **2** is consistent with similar Re(I) tricarbonyl diimine complexes with *S*-containing ancillary ligands.[61, 65]

Cytotoxicity and Cellular Localization

Cell Viability. The cytotoxicity of compounds **1**, **2** and cisplatin were assessed with the MDA-MB-231 breast cancer cell line using the alamarBlue cell viability assay and IC_{50} values were determined (Table 1); we previously discussed the data for **1** and cisplatin.[46] The results showed greater cytotoxicity for complex **1** (IC_{50} = 38 ± 6 μM) at 24 h, compared to both cisplatin and **2** (IC_{50} >100 μM) over the same time period. After 48 h the IC_{50} of **1** decreased to 26 ± 3 μM, whereas cisplatin was 11 ± 2 μM. When initially assessing the cytotoxicity of **2**, concentrations of up to 800 μM were used but minimal cytotoxicity was observed. The dose-response range was increased 10-fold in comparison to concentrations used for **1** and cisplatin. A concentration of over 1600 μM of compound **2** was cytostatic (cells were dead or not replicating). When comparing the dose-response curve for both complexes (Figure 3), it can be seen that cytotoxicity in **1** occurs at a much lower dosage in comparison to **2**. This indicates that the replacement of the aqua ligand in **1** with thiosulfate in **2** decreases its overall cytotoxicity, highlighting the importance of the nature of the ancillary ligand, and the overall charge of the complex.

Table 1. IC_{50} values of **1**, **2** and cisplatin against MDA-MB-231 breast cancer cells [a]

Complex	**IC_{50} (μM)**	
	24 Hours	**48 Hours**
1 [b]	38 ± 6	26 ± 3
2 [c]	>100	>100
Cisplatin [b]	>100	11 ± 2

[a] Data are represented as means ± standard deviations from three independent experiments with 9 biological replicates per concentration level. [b] From reference 46 . [c] This work.

The addition of STS has been demonstrated to counter the toxic side effects of cisplatin, which sometimes is a problematic aspect of chemotherapeutic treatments for multiple cancer types. We have shown that reaction of **1** with excess STS in aqueous solution leads to partial exchange of its coordinated water molecule with a thiosulfate ion, as in the crystal structure of (*fac*-$[Re(CO)_3(bpy)(H_2O)]$)(*fac*-$[Re(CO)_3(bpy)(S_2O_3)]$)·$4H_2O$ (**3**), and that the *fac*-$[Re(CO)_3(bpy)(S_2O_3)]^-$ anion in **2** has considerably lower toxicity than the *fac*-$[Re(CO)_3(bpy)(H_2O)]^+$ cation in **1**. If significant cytotoxic side effects are documented in future for *fac*-$[Re(CO)_3(bpy)(H_2O)]^+$ or similar *fac*-$[Re(CO)_3(N,N)(H_2O)]^+$ complexes, we would anticipate, given our results, that treatment with STS could be tested as a therapeutic option to counter any negative chemotherapeutic effects.

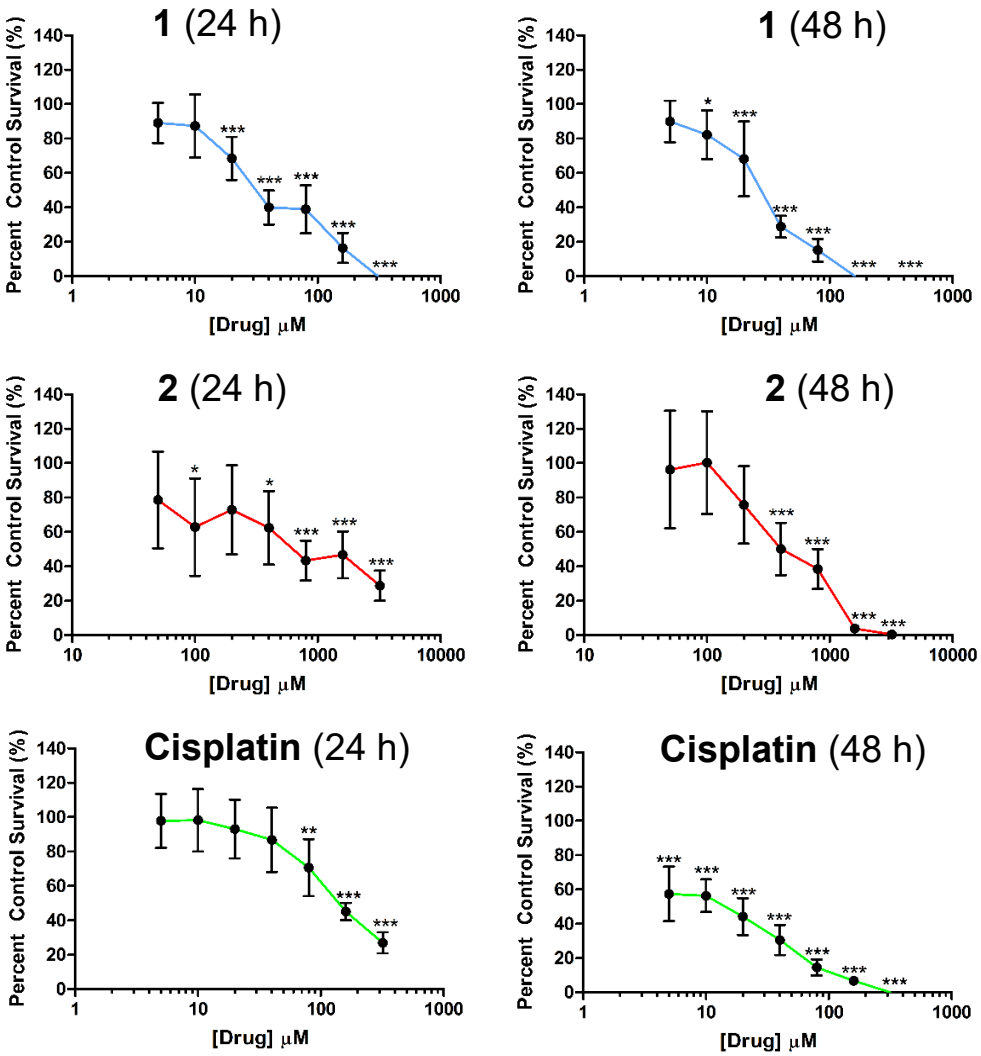

Figure 3. Cell viability data in MDA-MB-231 breast cancer cells when treated with **1**, **2** and cisplatin for 24 h and 48 h. Data are represented as means ± standard deviations from three independent experiments with 9 biological replicates per concentration level. Data were analyzed with a one-way ANOVA followed by Dunnet post-tests: *$p < 0.05$; ** $p < 0.01$; *** $p < 0.001$ from comparisons between treated and control cells. Data for **1** and cisplatin were adapted by permission from Springer: Capper, M. S. et al. Cytotoxicity, cellular localization and photophysical properties of Re(I) tricarbonyl complexes bound to cysteine and its derivatives. *J. Biol. Inorg. Chem.* **2020**, *25*, 759.[46]

Synchrotron-based X-ray Fluorescence Microscopy (XFM)

Cellular uptake and localization of the Re-complexes in **1** and **2** in MDA-MB-231 breast cancer cells were monitored using XFM. Comparison between the elemental distribution images in Figures 4, S5 (a-c), and the quantification histograms in Figure 5 shows a significant accumulation of Re in cells treated with the cationic complex from **1** as opposed to cells treated with the anionic complex in **2**. This indicates that replacing the aqua ligand in **1** with thiosulfate in **2** hinders its transportation into the cell, explaining the reduced cytotoxicity of **2** (IC_{50} > 100 μM; Table 1).

There are only a few studies in the literature on the toxicity of anionic *fac*-$[Re(CO)_3(N,N)(X)]^-$ complexes,[66] considering the internal net negative charge in healthy cells compared to the exterior, preventing uptake through passive diffusion.[67] The Coogan group studied membrane permeability for a series of cationic and anionic *fac*-$[Re(CO)_3(N,N)(X)]^{+/-}$ complexes, and found that *fac*-$[Re(CO)_3(N,N)(X)]^-$ containing a lipophilic ligand (*N,N*) = bathophenantroline disulfonate, and X = pyridine (Py) or Py-3-CH_2OH were membrane impermeable towards liposomes that were used as models for the cell membrane. Both complexes, however, accumulated in *Spironucleus vortens* cells but showed different cytotoxicity: the complex with X = hydroxymethylpyridine appeared to have low toxicity, while the one with simple pyridine was toxic.[68] Moreover, these anionic polar species displayed some level of association with MCF-7 cells, possibly interacting with cationic residues in the glycoprotein and glycolipid layer (the "glycocalyx"), or proteins of the extracellular matrix surrounding the plasma membrane, while a similar more lipophilic species with X = Py-$CH_2OCO(CH_2)_{12}CH_3$ showed no sign of uptake. The cationic complexes were generally taken up well through passive diffusion.[69] For example, the *fac*-$[Re(CO)_3(bpy)(3\text{-chloromethyl pyridyl})]^+$ cation was localized in the mitochondria.[70] Neutral complexes display relatively lower cellular uptake and toxicity.[46, 66, 71] Consequently changes in

the nature of the diimine (*N,N*) and the ancillary (X) ligands in *fac*-$[Re(CO)_3(L)(X)]^{-,0,+}$ complexes affecting their charge and lipophilicity, play an important role in their cellular uptake.

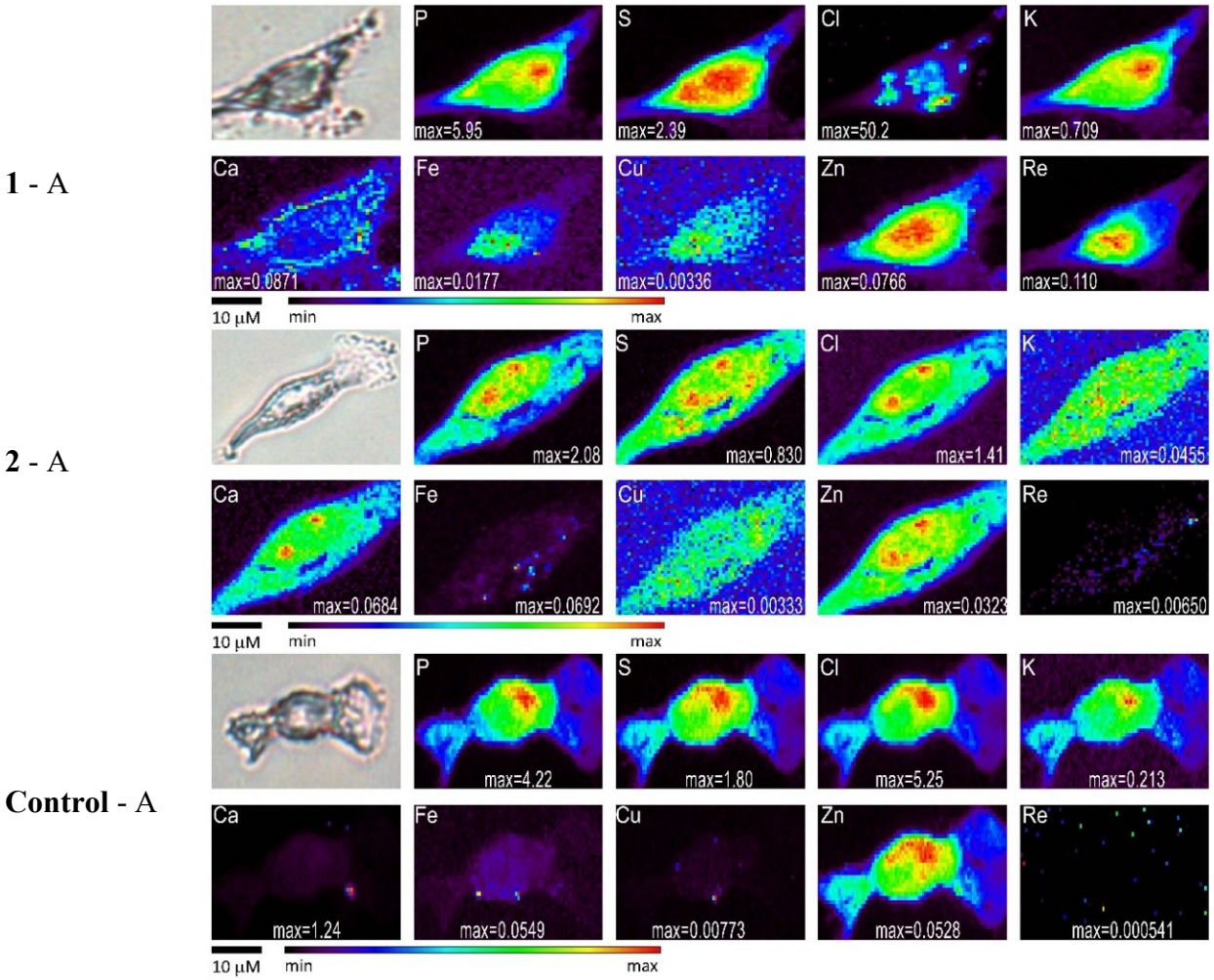

Figure 4. Optical micrographs (top left), and XFM elemental distribution map of MDA-MB-231 cells treated for 6 h with **1** (cell **1**-A), **2** (cell **2**-A) and DMEM (cell **Control**-A). The maximum elemental area densities (quantified from standards and expressed in µg cm^{-2}) are given in the bottom of each map.

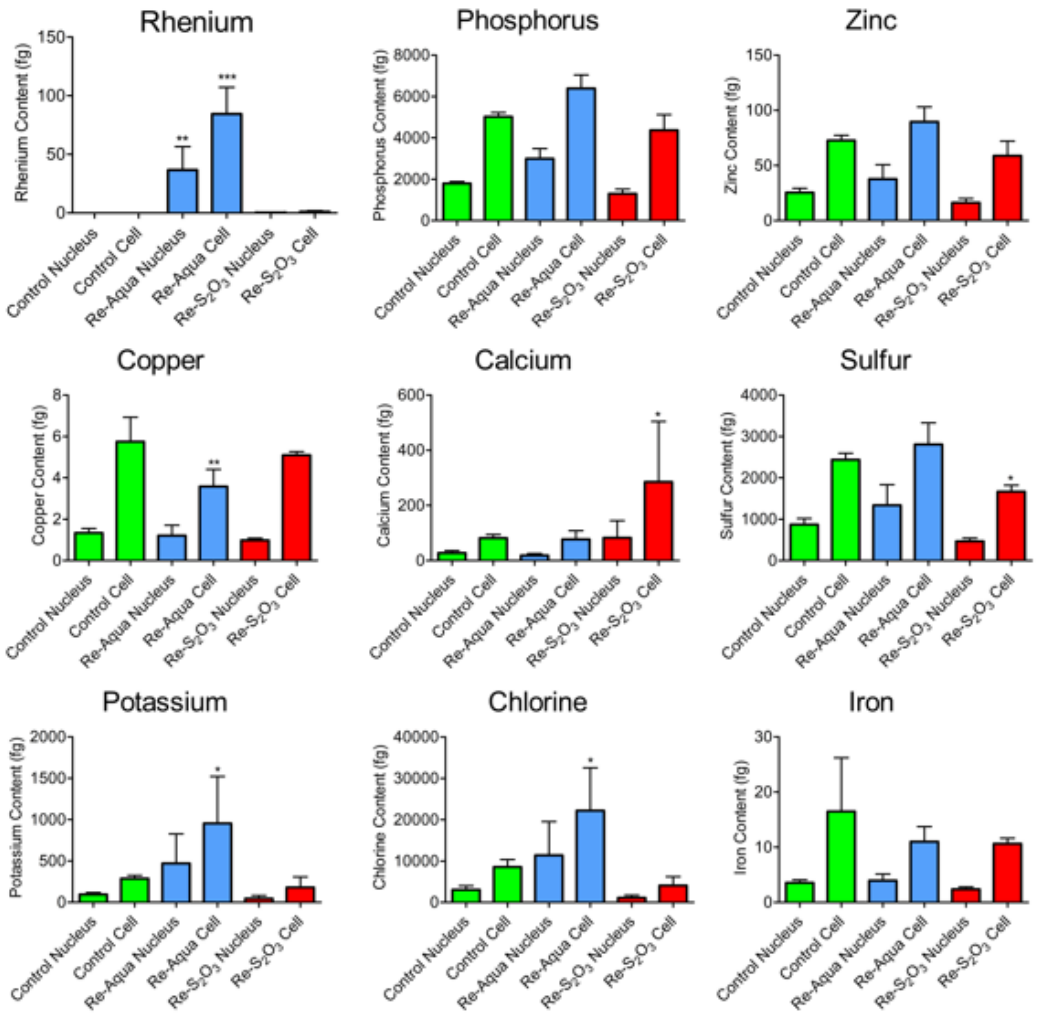

Figure 5. Intracellular content of P, S, Cl, K, Ca, Fe, Cu, Zn, and Re obtained by quantification using XFM as compared with the nuclear content of MDA-MB-231 cells treated for 6 h with control (green, n = 5) as well as 20 μM solutions of **1** (blue, n = 4) and **2** (red, n = 4) in DMEM. Error bars represent standard deviations. Data were analyzed with a one-way ANOVA followed by Tukey post-tests: *$p < 0.05$; ** $p < 0.01$; *** $p < 0.001$ from comparisons between treated and control cell/nucleus regions. The high Ca content in cells treated with **2** is assumed to be due to a single anomalous result in one cell, reflected in the large statistical difference. Data for control and **1** were adapted by permission from Springer: Capper, M. S. et al. Cytotoxicity, cellular localization and photophysical properties of Re(I) tricarbonyl complexes bound to cysteine and its derivatives. *J. Biol. Inorg. Chem.* **2020**, *25*, 759.[46]

Conclusion

Replacing the aqua ligand in *fac*-[$Re(CO)_3(bpy)(H_2O)$](CF_3SO_3) (**1**) with thiosulfate in Na(*fac*-[$Re(CO)_3(bpy)(S_2O_3)$]).H_2O (**2**), drastically reduces the cytotoxicity in MDA-MB-231 breast cancer cells. XFM images show high accumulation of the cationic complex *fac*-$[Re(CO)_3(bpy)(H_2O)]^+$ (of **1**) in areas outside the nucleus as well as localization with Zn inside the nucleus. In contrast, the cellular uptake of **2** was considerably less. We conclude that the negatively charged species *fac*-$[Re(CO)_3(bpy)(S_2O_3)]^-$ generated by coordination of thiosulfate to the $Re(CO)_3(bpy)^+$ core cannot easily pass through the cell membrane, thus preventing its cellular uptake. To the best of our knowledge, this is the second anticancer agent (after cisplatin) that is inhibited by thiosulfate. This finding could be of significant importance for potential use of sodium thiosulfate to minimize side effects of *fac*-$Re(CO)_3(N,N)^+$ based chemotherapeutics.

ASSCOCIATED CONTENT

Electronic Supplementary Information. Physical measurements and methods (NMR, FT-IR, ESI-MS, TG); crystal data, selected bond distances and bond angles for the compounds {Na(*fac*-[$Re(CO)_3(bpy)(S_2O_3)$])·1.75H_2O·C_2H_5OH}$_4$ (**2**·0.75H_2O·C_2H_5OH)$_4$ and (*fac*-[$Re(CO)_3(bpy)(H_2O)$]) (*fac*-[$Re(CO)_3(bpy)(S_2O_3)$])·4H_2O (**3**); survey of $Re(CO)_3^+$ complexes with an S-donor ligand in the Cambridge Structural Database (CSD); ^{13}C, ^1H NMR and FT-IR spectra of **1** and **2**; TG analysis, ESI-mass spectra and peak assignments for compound **2**; XFM elemental distribution map and XFM spectra of MDA-MB-231 cells treated with **1**, **2** or DMEM for 6 h.

Accession Codes

CCDC 2054796 and CCDC 2054797 contain the supplementary crystallographic data for this paper. These data can be obtained free of charge via www.ccdc.cam.ac.uk/data_request/cif, or by e-mailing data_request@ccdc.cam.ac.uk, or by contacting The Cambridge Crystallographic Data Centre, 12 Union Road, Cambridge CB2 1EZ, UK; fax: +44 1223 336033.

AUTHOR INFORMATION

Corresponding Author

* E-mail: faridehj@ucalgary.ca

Notes

There are no conflicts to declare.

ACKNOWLEDGEMENTS

We are grateful to Mr. Wade White at the instrumentation facility at the Department of Chemistry for assistance with the ESI-MS measurement. This work was financially supported by the Natural Science and Engineering Research Council of Canada (NSERC) funding reference number RGPIN 2016-04546 (FJ) and RGPIN 2018-04773 (CS), the Canadian Foundation for Innovation (CFI; #9479), the Province of Alberta (Department of Innovation and Science), and the Canadian Cancer Society (#300072). A.E.G acknowledges University of Calgary Eyes High, and Faculty of Science Dean's Open Competitions Doctoral Scholarships. X-ray fluorescence microscopy data were collected at the Advanced Photon Source (APS, Proposal No. 53103). Use of the Advanced Photon Source was supported by the U.S. Department of Energy, Office of Science, Office of Basic Energy Sciences, under contract No. DE-AC02-06CH11357.

ABBREVIATIONS

STS, sodium thiosulfate; ESI-MS, electrospray ionization mass spectrometry; XFM, X-ray fluorescence microscopy; bpy, 2,2′-bipyridine; phen, 1,10-phenanthroline; DMEM, Dulbecco's Modified Eagles Medium; PBS, phosphate buffered saline; IC_{50}, half-maximal inhibitory concentration.

References

1. B. Rosenberg, L. Van Camp and T. Krigas, *Nature*, 1965, **205**, 698-699.
2. A.-M. Florea and D. Büsselberg, *Cancers*, 2011, **3**, 1351-1371.
3. N. J. Wheate, S. Walker, G. E. Craig and R. Oun, *Dalton Trans.*, 2010, **39**, 8113-8127.
4. T. Makovec, *Radiol Oncol*, 2019, **53**, 148-158.
5. S. J. Berners-Price and T. G. Appleton, in *Platinum-Based Drugs in Cancer Therapy*, eds. L. R. Kelland and N. P. Farrell, Humana Press, Totowa, NJ, 2000, pp. 3-35.
6. M. S. Davies, S. J. Berners-Price and T. W. Hambley, *Inorg. Chem.*, 2000, **39**, 5603-5613.
7. A. I. Ivanov, J. Christodoulou, J. A. Parkinson, K. J. Barnham, A. Tucker, J. Woodrow and P. J. Sadler, *J. Biol. Chem.*, 1998, **273**, 14721-14730.
8. R. Marullo, E. Werner, N. Degtyareva, B. Moore, G. Altavilla, S. S. Ramalingam and P. W. Doetsch, *PLoS One*, 2013, **8**, e81162.
9. G. Laurell and P. Videhult Pierre, in *Free Radicals in ENT Pathology*, eds. J. Miller, C. G. Le Prell and L. Rybak, Springer International Publishing, Cham, 2015, DOI: 10.1007/978-3-319-13473-4_11, pp. 217-241.
10. M. Shea, J. A. Koziol and S. B. Howell, *Clin. Pharmacol. Ther.*, 1984, **35**, 419-425.
11. E. A. Neuwelt, R. E. Brummett, N. D. Doolittle, L. L. Muldoon, R. A. Kroll, M. A. Pagel, R. Dojan, V. Church, L. G. Remsen and J. S. Bubalo, *J. Pharmacol. Exp. Ther.*, 1998, **286**, 77.
12. K. T. Robbins, P. Kumar, F. S. H. Wong, W. F. Hartsell, P. Flick, R. Palmer, A. B. Weir III, H. B. Neill, T. Murry, R. Ferguson, C. Hanchett, F. Vieira, A. Bush and S. B. Howell, *Head Neck*, 2000, **22**, 687-693.
13. N. D. Doolittle, L. L. Muldoon, R. E. Brummett, R. M. Tyson, C. Lacy, J. S. Bubalo, D. F. Kraemer, M. C. Heinrich, J. A. Henry and E. A. Neuwelt, *Clin. Cancer Res.*, 2001, **7**, 493.
14. D. R. Freyer, L. Chen, M. D. Krailo, K. Knight, D. Villaluna, B. Bliss, B. H. Pollock, J. Ramdas, B. Lange, D. Van Hoff, M. L. VanSoelen, J. Wiernikowski, E. A. Neuwelt and L. Sung, *Lancet Oncol.*, 2017, **18**, 63-74.
15. P. R. Brock, R. Maibach, M. Childs, K. Rajput, D. Roebuck, M. J. Sullivan, V. Laithier, M. Ronghe, P. Dall'Igna, E. Hiyama, B. Brichard, J. Skeen, M. E. Mateos, M. Capra, A. A. Rangaswami, M. Ansari, C. Rechnitzer, G. J. Veal, A. Covezzoli, L. Brugières, G. Perilongo, P. Czauderna, B. Morland and E. A. Neuwelt, *N. Engl. J. Med.*, 2018, **378**, 2376-2385.
16. R. A. Hazlitt, J. Min and J. Zuo, *J. Med. Chem.*, 2018, **61**, 5512-5524.
17. D. Mukherjea, A. Dhukhwa, A. Sapra, P. Bhandari, K. Woolford, J. Franke, V. Ramkumar and L. Rybak, *Expert. Opin. Drug Metab. Toxicol.*, 2020, **16**, 965-982.

18. B. Erdlenbruch, A. Pekrun, H. Schiffmann, O. Witt and M. Lakomek, *Med. Pediatr. Oncol.*, 2002, **38**, 349-352.
19. J. Uozumi, M. Ishizawa, Y. Iwamoto and T. Baba, *Cancer Chemother. Pharmacol.*, 1984, **13**, 82-85.
20. M. Sooriyaarachchi, J. Gailer, N. V. Dolgova, I. J. Pickering and G. N. George, *J. Inorg. Biochem.*, 2016, **162**, 96-101.
21. M. Sooriyaarachchi, A. Narendran and J. Gailer, *Metallomics*, 2012, **4**, 960-967.
22. M. Sooriyaarachchi, G. N. George, I. J. Pickering, A. Narendran and J. Gailer, *Metallomics*, 2016, **8**, 1170-1176.
23. P. C. Bruijnincx and P. J. Sadler, *Curr. Opin. Chem. Biol.*, 2008, **12**, 197-206.
24. C. S. Allardyce, A. Dorcier, C. Scolaro and P. J. Dyson, *Appl. Organomet. Chem*, 2005, **19**, 1-10.
25. P. Collery, D. Desmaele and V. Vijaykumar, *Curr. Pharm. Des.*, 2019, **25**, 3306 - 3322.
26. K. Qiu, Y. Chen, T. W. Rees, L. Ji and H. Chao, *Coor. Chem. Rev.*, 2019, **378**, 66-86.
27. E. Villemin, Y. C. Ong, C. M. Thomas and G. Gasser, *Nat. Rev. Chem.*, 2019, **3**, 261-282.
28. J. Karges, S. Kuang, F. Maschietto, O. Blacque, I. Ciofini, H. Chao and G. Gasser, *Nat. Commun.*, 2020, **11**, 3262.
29. E. B. Bauer, A. A. Haase, R. M. Reich, D. C. Crans and F. E. Kühn, *Coor. Chem. Rev.*, 2019, **393**, 79-117.
30. A. Leonidova and G. Gasser, *ACS Chem. Biol.*, 2014, **9**, 2180-2193.
31. N. Viola-Villegas, A. E. Rabideau, J. Cesnavicious, J. Zubieta and R. P. Doyle, *Chem. Med. Chem.*, 2008, **3**, 1387-1394.
32. A. W.-T. Choi, M.-W. Louie, S. P.-Y. Li, H.-W. Liu, B. T.-N. Chan, T. C.-Y. Lam, A. C.-C. Lin, S.-H. Cheng and K. K.-W. Lo, *Inorg. Chem.*, 2012, **51**, 13289-13302.
33. A. Leonidova, V. Pierroz, L. A. Adams, N. Barlow, S. Ferrari, B. Graham and G. Gasser, *ACS Med. Chem. Lett.*, 2014, **5**, 809-814.
34. B. L. Murphy, S. C. Marker, V. J. Lambert, J. J. Woods, S. N. MacMillan and J. J. Wilson, *J. Organomet. Chem.*, 2020, **907**, 121064.
35. S. C. Marker, A. P. King, R. V. Swanda, B. Vaughn, E. Boros, S.-B. Qian and J. J. Wilson, *Angew. Chem. Int. Ed.*, 2020, **59**, 13391-13400.
36. S. C. Marker, A. P. King, S. Granja, B. Vaughn, J. J. Woods, E. Boros and J. J. Wilson, *Inorg. Chem.*, 2020, **59**, 10285-10303.
37. V. L. Gantsho, M. Dotou, M. Jakubaszek, B. Goud, G. Gasser, H. G. Visser and M. Schutte-Smith, *Dalton Trans.*, 2020, **49**, 35-46.
38. M. S. Capper, H. Packman and M. Rehkämper, *ChemBioChem*, 2020, **21**, 2111-2115.
39. I. Kitanovic, S. Can, H. Alborzinia, A. Kitanovic, V. Pierroz, A. Leonidova, A. Pinto, B. Spingler, S. Ferrari, R. Molteni, A. Steffen, N. Metzler-Nolte, S. Wölfl and G. Gasser, *Chem. Eur. J.*, 2014, **20**, 2496-2507.
40. A. Leonidova, V. Pierroz, R. Rubbiani, Y. Lan, A. G. Schmitz, A. Kaech, R. K. O. Sigel, S. Ferrari and G. Gasser, *Chem. Sci.*, 2014, **5**, 4044-4056.
41. C. C. Konkankit, A. P. King, K. M. Knopf, T. L. Southard and J. J. Wilson, *ACS Med. Chem. Lett.*, 2019, **10**, 822-827.
42. G. Kirker, S. Zelinka, S.-C. Gleber, D. Vine, L. Finney, S. Chen, Y. P. Hong, O. Uyarte, S. Vogt, J. Jellison, B. Goodell and J. E. Jakes, *Sci. Rep.*, 2017, **7**, 41798.
43. J. L. Wedding, H. H. Harris, C. A. Bader, S. E. Plush, R. Mak, M. Massi, D. A. Brooks, B. Lai, S. Vogt and M. V. Werrett, *Metallomics*, 2017, **9**, 382-390.

44. C. C. Konkankit, J. Lovett, H. H. Harris and J. J. Wilson, *Chem. Comm.*, 2020, **56**, 6515-6518.
45. K. M. Knopf, B. L. Murphy, S. N. MacMillan, J. M. Baskin, M. P. Barr, E. Boros and J. J. Wilson, *J. Am. Chem. Soc.*, 2017, **139**, 14302-14314.
46. M. S. Capper, A. Enriquez Garcia, N. Macia, B. Lai, J.-B. Lin, M. Nomura, A. Alihosseinzadeh, S. Ponnurangam, B. Heyne, C. S. Shemanko and F. Jalilehvand, *J. Biol. Inorg. Chem.*, 2020, **25**, 759-776.
47. D. B. G. Williams and M. Lawton, *J. Org. Chem.*, 2010, **75**, 8351-8354.
48. J. M. Smieja and C. P. Kubiak, *Inorg. Chem.*, 2010, **49**, 9283-9289.
49. B. Salignac, P. V. Grundler, S. Cayemittes, U. Frey, R. Scopelliti, A. E. Merbach, R. Hedinger, K. Hegetschweiler, R. Alberto and U. Prinz, *Inorg. Chem.*, 2003, **42**, 3516-3526.
50. SAINT *Bruker-AXS.*, Madison, Wisconsin, USA, 2017.
51. XPREP *Bruker-AXS.*, Madison, Wisconsin, USA, 2017.
52. O. V. Dolomanov, L. J. Bourhis, R. J. Gildea, J. A. Howard and H. Puschmann, *J. Appl. Crystallogr.*, 2009, **42**, 339-341.
53. G. M. Sheldrick, *Acta Crystallogr. A*, 2015, **71**, 3-8.
54. G. M. Sheldrick, *Acta Crystallogr. C: Struc. Chem.*, 2015, **71**, 3-8.
55. A. Enriquez Garcia, B. Lai, S. G. Gopinathan, H. H. Harris, C. S. Shemanko and F. Jalilehvand, *Chem. Comm.*, 2019, **55**, 8223-8226.
56. R. McRae, B. Lai and C. J. Fahrni, *Metallomics*, 2013, **5**, 52-61.
57. R. McRae, B. Lai, S. Vogt and C. J. Fahrni, *J. Struct. Biol*, 2006, **155**, 22-29.
58. P. Van Epsen, in *Handbook of X-ray Spectrometry: Methods and Techniques*, eds. R. E. Van Grieken and A. A. Markowicz, Marcel Dekker Inc., New York, 2nd edn., 2002, ch. 4, pp. 239 - 339.
59. S. Vogt, *J. Phys. IV*, 2003, **104**, 635-638.
60. E. A. Carter, B. S. Rayner, A. I. McLeod, L. E. Wu, C. P. Marshall, A. Levina, J. B. Aitken, P. K. Witting, B. Lai, Z. Cai, S. Vogt, Y. C. Lee, C. I. Chen, M. J. Tobin, H. H. Harris and P. A. Lay, *Mol. Biosyst.*, 2010, **6**, 1316-1322.
61. E. Hevia, J. Pérez, V. Riera and D. Miguel, *Organometallics*, 2003, **22**, 257-263.
62. S. E. Kabir, J. Alam, S. Ghosh, K. Kundu, G. Hogarth, D. A. Tocher, G. M. G. Hossain and H. W. Roesky, *Dalton Trans.*, 2009, 4458-4467.
63. L. Cuesta, D. C. Gerbino, E. Hevia, D. Morales, M. E. Navarro Clemente, J. Pérez, L. Riera, V. Riera, D. Miguel, I. del Río and S. García-Granda, *Chem. Eur. J.*, 2004, **10**, 1765-1777.
64. A. Vlček, in *Topics in Organometallic Chemistry: Photophysics of Organometallics*, ed. A. J. Lees, Springer - Verlag, Berlin, Heidelberg, 2010, pp. 73 - 114.
65. V. Fernández-Moreira and H. Sastre-Martín, *Inorg. Chim. Acta*, 2017, **460**, 127-133.
66. C. Otero, A. Carreño, R. Polanco, F. M. Llancalahuen, R. Arratia-Pérez, M. Gacitúa and J. A. Fuentes, *Front. Chem.*, 2019, **7**.
67. F. L. Thorp-Greenwood, R. G. Balasingham and M. P. Coogan, *J. Organomet. Chem.*, 2012, **714**, 12-21.
68. A. J. Amoroso, M. P. Coogan, J. E. Dunne, V. Fernández-Moreira, J. B. Hess, A. J. Hayes, D. Lloyd, C. Millet, S. J. Pope and C. Williams, *Chem. Comm.*, 2007, 3066-3068.
69. V. Fernández-Moreira, F. L. Thorp-Greenwood, A. J. Amoroso, J. Cable, J. B. Court, V. Gray, A. J. Hayes, R. L. Jenkins, B. M. Kariuki, D. Lloyd, C. O. Millet, C. F. Williams and M. P. Coogan, *Org. Biomol. Chem.*, 2010, **8**, 3888-3901.
70. A. J. Amoroso, R. J. Arthur, M. P. Coogan, V. Fernández-Moreira, A. J. Hayes, D. Lloyd, C. Millet and S. J. Pope, *New J. Chem.*, 2008, **32**, 1097-1102.

71. A. Carreño, E. Solís-Céspedes, C. Zúñiga, J. Nevermann, M. M. Rivera-Zaldívar, M. Gacitúa, A. Ramírez-Osorio, D. Páez-Hernández, R. Arratia-Pérez and J. A. Fuentes, *Chem. Phys. Lett.*, 2019, **715**, 231-238.